American Mineralogist, Volume 97, pages 257–261, 2012

Redetermination of the structure of 5*C* pyrrhotite at low temperature and at room temperature

David C. Liles[1] and Johan P.R. de Villiers[2,*]

[1]Department of Chemistry, University of Pretoria, Private Bag X20, Hatfield 0028, South Africa
[2]Department of Materials Science and Metallurgical Engineering, University of Pretoria, Private Bag X20, Hatfield 0028, South Africa

Abstract

The crystal structure of a 5*C* pyrrhotite from Silberberg Mine, Bodenmais, Germany, has been determined at 120 and 293 K in space group $P2_1$. The low-temperature structure refined to $R = 0.0261$ for 5727 data with $I_o > 2\sigma(I_o)$ and $R = 0.0354$ for all 7121 data. The room-temperature structure of the same crystal refined to $R = 0.0383$ for 2471 data with $I_o > 2\sigma(I_o)$ and $R = 0.0550$ for all 3419 data. In addition, the diffraction data of a 5*C* pyrrhotite crystal from Copper Cliff Mine, Sudbury, Canada, previously refined in space group *Cmce*, has been transformed and also refined in space group $P2_1$. This structure refined to $R = 0.0441$ for 2701 data with $I_o > 2\sigma(I_o)$ and $R = 0.0672$ for all 3843 data, which is a substantial improvement over the previous refinement.

The structure is characterized by iron vacancy avoidance within a layer, and with partially occupied sites projecting on top of each other in adjacent layers. Two half-occupied sites and two sites each with occupancy of 0.88 are present in the Bodenmais structure, together with one site with occupancy of 0.28. The distribution in the crystal from Sudbury is slightly different and cannot be described with the same number of partially occupied sites. Broadly, however, the two structures are similar.

Introduction

The crystal structure and vacancy distribution of 5*C* pyrrhotite (Fe_9S_{10}) have been the subjects of several studies, with the postulated structures mainly based on the structure of 4*C* pyrrhotite. These investigations attempted to predict the structure based on the arrangement of layers containing fully occupied iron sites and layers containing either two vacancies in 8 atom sites or one vacancy in 8 sites. The reader is referred to a comprehensive review by Elliott (2010). No crystal-structure determinations accompanied these postulated vacancy arrangements except for the above-mentioned author who attempted structure verification using synchrotron powder XRD data. More specifically, on the basis of vacancy avoidance Elliott (2010) proposed a structure for 5*C* pyrrhotite, which included the stacking of half-occupied and fully occupied iron sites. He postulated two equivalent arrangements of fully occupied and half-occupied sites, FA½A½B½B½FD½D½C½C½ and FA½A½B½B½FC½C½D½D½, where the A, B, C, and D arrangements are defined as corresponding to the vacancy arrangements in 4*C* pyrrhotite, and F a fully occupied layer. The vacancy arrangements in these layers (nomenclature of Wang and Salveson 2005) are shown in Figure 1. Note that the nomenclature of Wang and Salveson (2005) differs from that of Elliott (2010) in that the A-layer and D-layer of the former authors are interchanged in the latter.

The crystal structure of a 5*C* pyrrhotite from Copper Cliff Mine, Sudbury, Canada, was described by de Villiers et al. (2009) in the orthorhombic space group *Cmce* with a rather high *R*-factor of 0.072. If an iron site with partial occupancy of ~0.13 is included in the refinement, then the *R*-factor decreases to 0.060 for all observed data. The latter atomic site was not included in the published structure. Subsequently, the 5*C* structure was reexamined by Elliott (2010) who questioned the vacancy distribution of this structure and postulated a monoclinic structure in space group $P2_1/c$ and the vacancy distributions consisting of

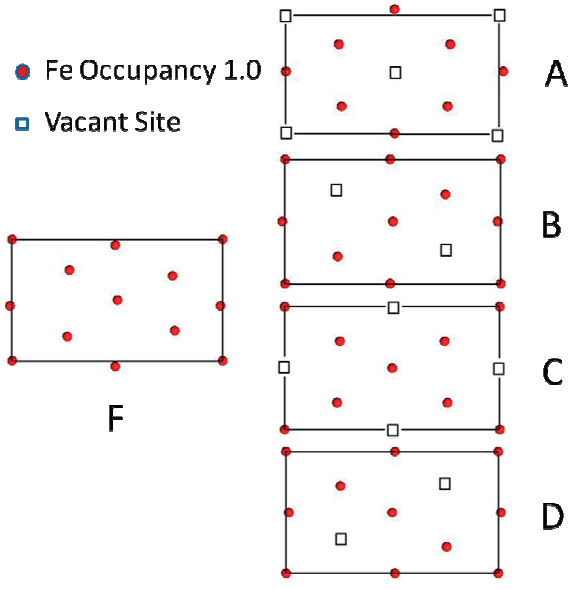

Figure 1. Distribution of vacancies in the A, B, C, and D cation layers of the 4C pyrrhotite structure, shown together with a layer with all cation sites filled, (F).

* E-mail: johan.devilliers@up.ac.za

0003-004X/12/0203–257$05.00/DOI: http://dx.doi.org/10.2138/am.2012.3887

fully occupied and half-occupied iron sites as described above. As a result, the structure of 5*C* pyrrhotite was reexamined in this study to resolve the differences in the structures proposed by these authors.

Experimental methods

Two crystals were selected for structure determination and refinement. The first was from Bodenmais, Germany, and is labeled "Pyrrhotite Silberberg mine, Bodenmais, (Bavaria, Germany), ex coll. University of Jena, HG12129." The crystal was mounted on a glass fiber and data were collected at 293 K on a Bruker (Siemens) P4 diffractometer equipped with a Bruker SMART 1 K CCD detector using graphite-crystal monochromated Mo$K\alpha$ radiation by means of a combination of φ and ω scans. Data reduction was performed using SAINT+ (Bruker 2001) and the intensities were corrected for absorption by multiple scans of symmetry equivalent reflections using SADABS (Bruker 2001).

Structure determination is complicated in that the unit cell can be described as orthorhombic, hexagonal, or monoclinic because of the fact that the unit-cell angular dimensions are so close to 90° or 120°, respectively, depending on the choice of the unit cell. In the monoclinic setting, six different possible unit-cell choices needed to be tested to obtain the correct setting for successful structure determination and for the comparison of structures obtained from different data sets. As the symmetry is close to hexagonal (only the distribution of certain partially occupied Fe sites breaks this higher symmetry), the monoclinic *a* and *c* axes and the lengths of the *ac* face diagonals are all very similar and the angle between any pair of these vectors is close to 120°. Thus, with judicial use of negative directions to maintain obtuse β angles and right-handed axes sets, the following six axis combinations need to be considered: *a*, *b*, *c*; *c*, –*b*, *a*; *a*, –*b*, –*ac*; *ac*, *b*, –*a*; *ac*, –*b*, *c*; *c*, *b*, –*ac*.

The structure was solved by direct methods using SHELXTS (Bruker 2001) and refined anisotropically by full-matrix least squares using SHELXTL (Bruker 2001) and SHELXL-97 (Sheldrick 2008). To lessen the correlation between iron site occupancies and thermal effects as reflected in the atomic displacement parameters, low-temperature data were collected using the same crystal at 120 K on an Oxford Diffraction (Agilent Technologies) SuperNova diffractometer using multi-layer X-ray optic monochromated Mo$K\alpha$ radiation by means of ω scans. A full sphere of data was collected. Data reduction was performed using CrysAlisPro (Oxford Diffraction 2010) and the intensities were corrected for absorption by CrysAlisPro using analytical numeric absorption methods employing a multifaceted crystal model based on expressions derived by Clark and Reid (1995).

The data for the second crystal from Sudbury were collected previously (de Villiers et al. 2009) at 293 K on a Bruker (Siemens) P4 diffractometer.

The crystals were then analyzed using a Cameca SX100 electron microprobe at the University of Pretoria, run at 20 kV accelerating voltage and 20 nA probe current using troilite as a standard for both iron and sulfur. The standard deviations in the Fe contents, expressed as a fraction of the formula Fe_9S_{10}, are given in Table 1.

Results

Refinement of the Bodenmais crystal in the orthorhombic space group *Cmce* (de Villiers et al. 2009) was not successful. However, by transforming the 293 K data to a monoclinic setting, a solution was obtained in the space group $P2_1$. In this structure five sites were refined with occupancies less than unity. The low-temperature data were refined using SHELXL-97 after transforming the unit cell to conform to the room-temperature structure and using that solution as a starting point.

For the Sudbury crystal, the primary diffraction data, which had been refined in space group *Cmce*, was transformed to a monoclinic setting and refined anisotropically in space group $P2_1$ to $R = 0.0441$ for 2701 data with $I_o > 2\sigma(I_o)$ and 0.0672 for all 3843 data, a substantial improvement over the previous refinement in the orthorhombic setting with $R = 0.060$. In this case the occupancies of seven sites were refined, although some

Table 1. Crystal data and structure refinement for 5*C* pyrrhotites

Locality	Bodenmais	Bodenmais	Sudbury
Temperature	120 K	293 K	293 K
Calculated formula	$Fe_{9.017}S_{10}$	$Fe_{9.021}S_{10}$	$Fe_{9.007}S_{10}$
Analyzed formula	$Fe_{9.010}S_{10}$	$Fe_{9.010}S_{10}$	$Fe_{9.014}S_{10}$
Analytical uncertainty (Fe)	$Fe_{0.035}$		$Fe_{0.031}$
Formula weight (atomic mass units)	824.30	824.52	823.71
Wavelength (Å)	0.71073	0.71073	0.71073
Crystal system	monoclinic	monoclinic	monoclinic
Space group	$P2_1$	$P2_1$	$P2_1$
a (Å)	6.8673(4)	6.8984(13)	6.893(3)
b (Å)	28.6536(9)	28.695(5)	28.643(12)
c (Å)	6.8592(4)	6.8915(13)	6.899(3)
β (°)	119.975(7)	119.956(2)	120.048(6)
Volume (Å^3)	1169.18(10)	1181.9(4)	1179.0(8)
Z	4	4	4
Density, calculated (Mg/m^3)	4.683	4.634	4.640
Absorption coefficient (mm^{-1})	12.586	12.456	12.468
F(000)	1579	1579	1576
Crystal size (mm^3)	0.139 x 0.103 x 0.063	0.139 x 0.103 x 0.063	0.14 x 0.06 x 0.03
Theta range for data collection	2.84 to 30.54°	2.84 to 26.55°	2.84 to 26.34°
Index ranges	$-9 \le h \le 9, -40 \le k \le 40, -9 \le l \le 9$	$-6 \le h \le 8, -20 \le k \le 35, -8 \le l \le 7$	$-3 \le h \le 8, -33 \le k \le 29, -8 \le l \le 7$
Reflections collected	28580	6341	6369
Independent reflections	7121 (R_{int} = 0.0207)	3419 (R_{int} = 0.0334)	3843 (R_{int} = 0.0243)
Completeness	99.9% to theta = 30.54°	99.2% to theta = 25.00°	98.7% to theta = 25.00°
Absorption correction	Analytical	Semi-empirical from equivalents	Semi-empirical from equivalents
Max. and min. transmission	0.525 and 0.288	0.456 and 0.310	0.688 and 0.389
Refinement method	Full-matrix least-squares on F^2	Full-matrix least-squares on F^2	Full-matrix least-squares on F^2
Data/restraints/parameters	7121/1/368	3419/1/368	3843/1/370
Goodness-of-fit on F^2	1.187	1.146	1.242
R_1 [$I_o > 2\sigma(I_o)$]	0.0261	0.0383	0.0441
wR_2 [$I_o > 2\sigma(I_o)$]	0.0527	0.1021	0.1174
R_1 (all data)	0.0354	0.0550	0.0672
wR_2 (all data)	0.0574	0.1138	0.1302
Absolute structure parameter	0.47(4)	0.43(5)	0.41(12)
Extinction coefficient	0.00045(2)	0.00021(7)	0.00019(5)
Largest diff. peak and hole (e·Å^{-3})	0.866 and –0.746	0.770 and –0.840	0.838 and –0.994

were close to unity. This gave a lower *R* factor and corresponded closer to the analyzed composition.

The crystal data for the three data sets are given in Table 1. The atomic positions, occupancies, and equivalent atomic displacement factors of the 120 and 293 K data for the crystal from Bodenmais and the 293 K data for the crystal from Sudbury are given in Tables 2, 3, and 4.

Because of the many unique octahedra, detailed bond lengths and angles, as well as anisotropic atomic displacement parameters, are not given here. These can however be obtained from the CIF files available on deposit[1] or from the authors.

A characteristic of the 5*C* structure from Bodenmais is the presence of 5 partially occupied sites in all the layers, with the following occupancies (Table 2, 120 K data); Fe2: 0.500(3), Fe9: 0.496(3), Fe12: 0.877(3), Fe14: 0.878(3), and Fe19: 0.283(2). The occupancies as determined from the 120 K data are presumed to be more precise than the 293 K data. At low temperature, the effect of the correlation between the smaller ADP values and the occupancies is reduced. The apparent difference in the occupancies in the same crystal at different temperatures is

TABLE 2. Atomic coordinates, occupancies, and equivalent isotropic displacement parameters (Å²) for the Bodenmais 5*C* pyrrhotite 120 K data

	x	y	z	Occupancy	U_{eq}
Fe1	0.46648(19)	0.21539(5)	0.7509(3)	1.0	0.0084(2)
Fe2	0.0001(5)	−0.09022(8)	0.7288(5)	0.500(3)	0.0099(5)
Fe3	0.5014(4)	0.11532(6)	0.7334(3)	1.0	0.0141(2)
Fe4	0.0191(3)	−0.08458(5)	0.2765(2)	1.0	0.0110(2)
Fe5	−0.0113(2)	0.01172(4)	0.76610(19)	1.0	0.0097(2)
Fe6	0.5269(3)	0.31543(5)	0.7506(3)	1.0	0.0108(2)
Fe7	−0.03518(18)	0.01518(5)	0.2126(2)	1.0	0.0093(2)
Fe8	0.9841(3)	0.31513(5)	0.7582(3)	1.0	0.0101(2)
Fe9	0.0038(5)	−0.17982(8)	0.7731(5)	0.496(3)	0.0084(5)
Fe10	−0.4702(2)	0.01493(4)	0.7818(2)	1.0	0.0075(2)
Fe11	0.4744(3)	−0.08539(5)	0.7246(3)	1.0	0.0095(2)
Fe12	0.5083(2)	0.01958(5)	0.2333(2)	0.877(3)	0.0086(3)
Fe13	0.0110(4)	0.11568(6)	0.2556(4)	1.0	0.0128(2)
Fe14	0.4937(2)	0.21045(5)	0.2252(3)	0.878(3)	0.0098(3)
Fe15	0.01268(19)	0.21833(4)	0.2772(3)	1.0	0.0090(2)
Fe16	0.03225(17)	0.21504(4)	0.7466(3)	1.0	0.0080(2)
Fe17	0.4970(3)	−0.18685(5)	0.7388(4)	1.0	0.0129(3)
Fe18	−0.0118(4)	0.11425(5)	0.7441(3)	1.0	0.0119(2)
Fe19	0.4964(11)	0.1149(2)	0.2644(8)	0.283(2)	0.0159(10)
Fe20	−0.5049(3)	−0.08322(5)	0.2569(3)	1.0	0.0126(3)
S1	0.3310(2)	−0.02954(6)	0.4159(3)	1.0	0.0039(3)
S2	0.3322(2)	−0.03473(7)	0.9162(3)	1.0	0.0053(3)
S3	−0.1623(2)	0.16557(8)	0.4176(2)	1.0	0.0049(3)
S4	0.1645(2)	−0.13736(8)	0.5816(3)	1.0	0.0067(3)
S5	−0.1712(2)	−0.04062(7)	0.9167(3)	1.0	0.0061(3)
S6	−0.1697(2)	−0.03387(7)	0.4155(3)	1.0	0.0049(3)
S7	0.6690(2)	0.26050(7)	0.5852(2)	1.0	0.0058(3)
S8	0.3320(2)	0.16087(8)	0.9126(2)	1.0	0.0071(3)
S9	0.1629(3)	0.06521(7)	0.0804(3)	1.0	0.0052(3)
S10	0.1641(3)	0.06239(8)	0.5809(3)	1.0	0.0057(3)
S11	0.3337(2)	0.16702(8)	0.4153(2)	1.0	0.0054(3)
S12	0.6688(3)	0.26564(7)	0.0844(2)	1.0	0.0057(3)
S13	0.1688(3)	0.26496(7)	0.0849(2)	1.0	0.0044(3)
S14	−0.3378(2)	−0.13449(9)	0.0812(3)	1.0	0.0056(3)
S15	0.1709(2)	0.27156(7)	0.5879(2)	1.0	0.0033(3)
S16	0.8355(2)	0.16862(8)	0.9169(2)	1.0	0.0049(3)
S17	0.1646(2)	−0.13160(8)	0.0833(3)	1.0	0.0056(3)
S18	−0.3416(2)	−0.13465(8)	0.5790(3)	1.0	0.0058(3)
S19	0.6674(3)	0.07015(8)	0.0801(3)	1.0	0.0046(3)
S20	0.6658(3)	0.06412(8)	0.5815(3)	1.0	0.0052(3)

Note: U_{eq} is defined as one third of the trace of the orthogonalized U_{ij} tensor.

TABLE 3. Atomic coordinates, occupancies, and equivalent isotropic displacement parameters (Å²) for the Bodenmais 5*C* pyrrhotite 293 K data

	x	y	z	Occupancy	U_{eq}
Fe1	0.4673(4)	0.21543(10)	0.7474(6)	1.0	0.0157(5)
Fe2	−0.0013(12)	−0.0902(2)	0.7299(13)	0.468(6)	0.0138(14)
Fe3	0.5023(9)	0.11471(12)	0.7378(7)	1.0	0.0197(5)
Fe4	0.0169(7)	−0.08520(10)	0.2739(6)	1.0	0.0175(7)
Fe5	−0.0115(5)	0.01159(9)	0.7638(5)	1.0	0.0179(7)
Fe6	0.5246(6)	0.31557(10)	0.7491(6)	1.0	0.0183(6)
Fe7	−0.0312(5)	0.01524(10)	0.2148(5)	1.0	0.0144(6)
Fe8	0.9873(7)	0.31511(11)	0.7594(6)	1.0	0.0158(6)
Fe9	0.0040(11)	−0.18036(19)	0.7728(11)	0.484(6)	0.0122(13)
Fe10	−0.4724(5)	0.01479(10)	0.7775(5)	1.0	0.0152(6)
Fe11	0.4774(6)	−0.08521(9)	0.7286(6)	1.0	0.0160(6)
Fe12	0.5061(5)	0.01973(12)	0.2355(6)	0.914(6)	0.0146(8)
Fe13	0.0084(8)	0.11612(12)	0.2538(9)	1.0	0.0199(5)
Fe14	0.4979(5)	0.21004(12)	0.2322(7)	0.891(6)	0.0160(9)
Fe15	0.0139(4)	0.21795(10)	0.2767(6)	1.0	0.0151(6)
Fe16	0.0278(4)	0.21488(9)	0.7464(6)	1.0	0.0133(5)
Fe17	0.4978(6)	−0.18681(10)	0.7408(8)	1.0	0.0178(7)
Fe18	−0.0092(8)	0.11418(11)	0.7426(6)	1.0	0.0176(5)
Fe19	0.496(3)	0.1140(6)	0.249(2)	0.285(7)	0.046(3)
Fe20	−0.5050(6)	−0.08340(10)	0.2558(7)	1.0	0.0178(7)
S1	0.3321(5)	−0.02985(13)	0.4157(5)	1.0	0.0080(7)
S2	0.3328(5)	−0.03387(13)	0.9166(6)	1.0	0.0079(8)
S3	−0.1617(5)	0.16582(13)	0.4170(5)	1.0	0.0089(8)
S4	0.1646(5)	−0.13731(15)	0.5816(6)	1.0	0.0088(8)
S5	−0.1710(5)	−0.04002(13)	0.9160(6)	1.0	0.0086(8)
S6	−0.1700(5)	−0.03363(14)	0.4149(6)	1.0	0.0086(8)
S7	0.6695(5)	0.26188(14)	0.5847(5)	1.0	0.0103(8)
S8	0.3329(6)	0.16174(14)	0.9116(6)	1.0	0.0104(8)
S9	0.1624(6)	0.06589(14)	1.0805(6)	1.0	0.0099(8)
S10	0.1650(6)	0.06309(15)	0.5804(5)	1.0	0.0095(8)
S11	0.3347(5)	0.16595(15)	0.4160(6)	1.0	0.0098(8)
S12	0.6694(6)	0.26559(14)	0.0843(5)	1.0	0.0088(7)
S13	1.1690(5)	0.26462(14)	0.0851(5)	1.0	0.0079(7)
S14	−0.3377(5)	−0.13384(13)	0.0818(6)	1.0	0.0095(8)
S15	0.1697(5)	0.27155(12)	0.5864(5)	1.0	0.0072(8)
S16	0.8358(5)	0.16902(14)	0.9161(5)	1.0	0.0074(7)
S17	0.1650(5)	−0.13208(15)	0.0833(6)	1.0	0.0101(8)
S18	−0.3416(5)	−0.13414(13)	0.5782(6)	1.0	0.0084(8)
S19	0.6670(6)	0.06920(15)	0.0799(6)	1.0	0.0107(8)
S20	0.6652(6)	0.06460(15)	0.5811(5)	1.0	0.0089(8)

Note: U_{eq} is defined as one third of the trace of the orthogonalized U_{ij} tensor.

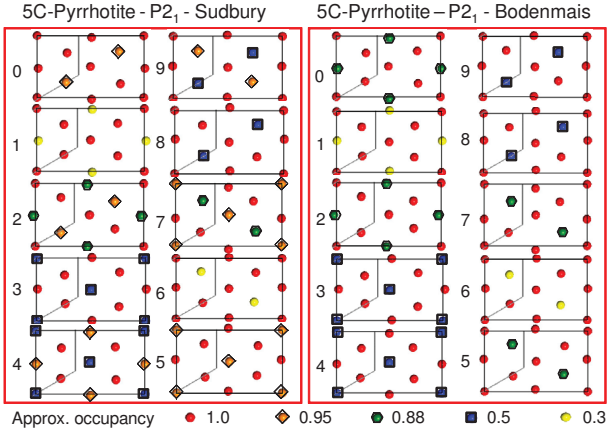

FIGURE 2. Distribution of iron sites in the Sudbury and Bodenmais structures. Part of the monoclinic cell is shown. The occupancies of the partially occupied sites are approximate and are given in the legend as different shaped and contrasted symbols.

[1] Deposit item AM-12-007, CIF files. Deposit items are available two ways: For a paper copy contact the Business Office of the Mineralogical Society of America (see inside front cover of recent issue) for price information. For an electronic copy visit the MSA web site at http://www.minsocam.org, go to the American Mineralogist Contents, find the table of contents for the specific volume/issue wanted, and then click on the deposit link there.

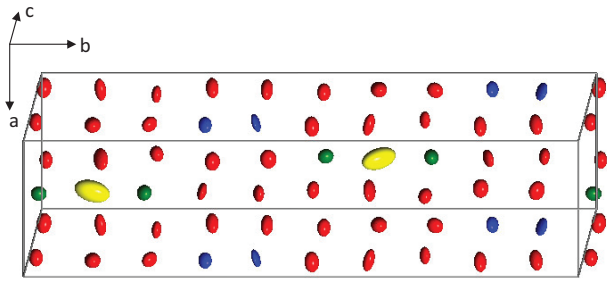

FIGURE 3. Distribution of iron sites in 5*C* pyrrhotite from Bodenmais. Opposite from the site with occupancy 0.28 (yellow) are two sites with occupancy ~0.88 (green), and two sites with occupancy 0.5 (blue) are adjacent.

therefore an artifact. The partially occupied sites are arranged as shown in Figure 2.

In this case, groups of three layers (layers 0,1,2 and 5,6,7) and two layers (3,4 and 8,9) contain vacancies that project directly on top of each other along the **b**-axis. From Figure 2, it can be deduced that the vacancy arrangement can be described in terms of the A, B, C, and D vacancy arrangements (Wang and Salveson 2005), rounded to two decimals as: $C_{0.88}C_{0.28}C_{0.88}D_{0.50}D_{0.50}B_{0.88}B_{0.28}B_{0.88}A_{0.50}A_{0.50}$. In each layer there are also three fully occupied sites per formula unit or six per unit cell. This relates to a composition of $Fe_{9.017}S_{10}$ as compared to a measured composition of $Fe_{9.010}S_{10}$.

It can also be seen from Figure 2 that two layers with half-occupied sites group together and that layers containing sites with occupancies of 0.88, 0.28, and 0.88 group together. This can be better seen in Figure 3.

The vacancy distribution in the 6*C* pyrrhotite structure (de Villiers and Liles 2010) is analogous to the 5*C* structure in that in addition to the half-occupied sites, there are also two other sites with occupancies of 0.87 and 0.90 as refined. Their distribution is however different in that these latter two sites in 6*C* pyrrhotite do not project on top of each other.

The vacancy distribution within layers is shown in Figure 4 for layer 1 and 3 of the Bodenmais structure. It is clear that the partially occupied sites are arranged so that vacancy avoidance is maintained within the layers, i.e., the partially occupied sites

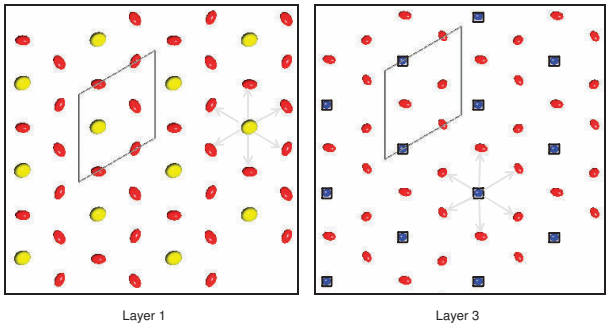

FIGURE 4. Distribution of filled iron sites around sites with partial occupancy for the sample of 5*C* pyrrhotite from Bodenmais. The Fe19 site in layer 1 has an occupancy of 0.28 and the Fe9 site in layer 3 an occupancy of 0.5. No two partially occupied sites are adjacent. Symbols are similar to Figure 2.

TABLE 4. Atomic coordinates, occupancies, and equivalent isotropic displacement parameters (Å²) for the Sudbury 5*C* pyrrhotite 293 K data

	x	y	z	Occupancy	U_{eq}
Fe1	0.4713(6)	0.21548(14)	0.7487(7)	1.0	0.0149(8)
Fe2	0.0019(10)	−0.0884(3)	0.7298(10)	0.475(9)	0.0115(15)
Fe3	0.5093(10)	0.11557(19)	0.7488(8)	1.0	0.0221(7)
Fe4	0.0184(7)	−0.08468(16)	0.2721(6)	1.0	0.0181(8)
Fe5	−0.0109(8)	0.01168(17)	0.7573(8)	0.938(7)	0.0266(12)
Fe6	0.5255(8)	0.31572(16)	0.7502(7)	1.0	0.0244(10)
Fe7	−0.0324(7)	0.01501(14)	1.2167(7)	1.0	0.0177(7)
Fe8	0.9875(8)	0.31558(16)	0.7637(7)	1.0	0.0228(9)
Fe9	0.0026(8)	−0.1806(2)	0.7670(9)	0.598(9)	0.0137(13)
Fe10	−0.4744(7)	0.01473(15)	0.7793(7)	1.0	0.0177(8)
Fe11	0.4762(6)	−0.08504(16)	0.7254(7)	0.950(7)	0.0161(9)
Fe12	0.5073(6)	0.01924(15)	0.2395(6)	1.0	0.0187(9)
Fe13	0.0019(9)	0.11622(18)	0.2397(9)	1.0	0.0212(7)
Fe14	0.5015(7)	0.20993(17)	0.2357(10)	0.803(9)	0.0199(13)
Fe15	0.0133(5)	0.21822(14)	0.2770(7)	1.0	0.0156(8)
Fe16	1.0260(6)	0.21483(15)	0.7422(8)	0.947(9)	0.0142(9)
Fe17	0.4998(6)	−0.18629(15)	0.7462(8)	1.0	0.0183(9)
Fe18	−0.0115(8)	0.11473(17)	0.7447(7)	1.0	0.0155(6)
Fe19	0.529(4)	0.1197(7)	1.272(4)	0.302(11)	0.114(9)
Fe20	−0.5093(6)	−0.08262(15)	0.2597(6)	1.0	0.0184(9)
S1	0.3305(6)	−0.0301(2)	0.4160(7)	1.0	0.0090(10)
S2	0.3305(6)	−0.0347(2)	0.9154(7)	1.0	0.0109(10)
S3	−0.1612(6)	0.1651(2)	0.4158(7)	1.0	0.0106(10)
S4	0.1649(6)	−0.1376(2)	0.5813(7)	1.0	0.0107(11)
S5	−0.1694(7)	−0.0402(2)	0.9151(7)	1.0	0.0119(12)
S6	−0.1693(7)	−0.0344(2)	0.4143(7)	1.0	0.0101(9)
S7	0.6696(7)	0.2612(2)	0.5851(8)	1.0	0.0140(12)
S8	0.3326(7)	0.1613(2)	0.9145(8)	1.0	0.0136(11)
S9	0.1613(7)	0.0650(2)	1.0768(8)	1.0	0.0127(10)
S10	0.1664(7)	0.0630(3)	0.5802(8)	1.0	0.0145(11)
S11	0.3355(7)	0.1656(2)	0.4171(8)	1.0	0.0125(10)
S12	0.6676(7)	0.2650(2)	1.0847(8)	1.0	0.0110(11)
S13	1.1717(7)	0.2640(2)	1.0857(8)	1.0	0.0101(11)
S14	−0.3386(6)	−0.1342(2)	0.0810(8)	1.0	0.0123(10)
S15	0.1703(7)	0.27065(19)	0.5876(8)	1.0	0.0086(11)
S16	0.8364(6)	0.1686(2)	0.9153(7)	1.0	0.0081(9)
S17	0.1650(6)	−0.1324(2)	1.0829(8)	1.0	0.0123(10)
S18	−0.3403(6)	−0.1347(2)	0.5805(8)	1.0	0.0115(10)
S19	0.6683(7)	0.0689(2)	1.0816(7)	1.0	0.0135(11)
S20	0.6663(7)	0.0643(2)	0.5838(8)	1.0	0.0122(10)

Note: U_{eq} is defined as one third of the trace of the orthogonalized U_{ij} tensor.

are surrounded by fully occupied sites. Between the layers, the partially occupied sites always project on top of each other. Since the sum of the occupancies of the group of 3 partially occupied sites approximates 2 and that of the group of 2 sites equals 1, there is no necessity for there ever to be more than 1 vacancy within any particular instance of either of these groups. Thus vacancy avoidance can also be maintained between layers, albeit in a disordered fashion.

From the refinement of a full sphere of single-crystal data to an R factor of 0.0261 at low temperature, it can be concluded that the structure postulated by Elliott (2010) is not supported by our structure determination. He predicted the structure to consist exclusively of half-occupied and fully occupied sites, with two equivalent arrangements, FA½A½B½B½FD½D½C½C½ and FA½A½B½B½FC½C½D½D½. The structure refined here contains sites with occupancies of 0.28 and 0.88 in addition to half-occupied sites with the distribution $C_{0.88}C_{0.28}C_{0.88}A_{0.50}A_{0.50}B_{0.88}B_{0.28}B_{0.88}D_{0.50}D_{0.50}$, using his notation.

The vacancy distribution in the Sudbury crystal is different from the Bodenmais one in that the Fe12 site refined to a fully occupied site in contrast to a site with occupancy of 0.88 in the latter crystal. The refinement was done with the inclusion of seven partially occupied sites distributed between all the layers,

with the following occupancies (Table 4): Fe2: 0.475(9), Fe5: 0.938(7), Fe9: 0.598(9), Fe11: 0.950(7), Fe14: 0.803(9), Fe16: 0.947(9), and Fe19: 0. 302(11). This arrangement gave the best correspondence to the composition as measured by electron microprobe, $Fe_{9.007}S_{10}$ as compared to an analyzed composition of $Fe_{9.014}S_{10}$. The occupancies of the different layers are graphically shown in Figure 2.

Refinement of the data with only four partially occupied sites (Fe2, Fe9, Fe14, and Fe19) resulted in a slightly higher *R* factor (0.046) and with a calculated composition of $Fe_{9.109}S_{10}$, showing a larger deviation from the analyzed composition.

Discussion

The structures described here were refined to acceptably low *R* factors using the low-temperature (120 K) data of the full reflection sphere as basis. They prove that the vacancy distribution of partially occupied iron sites in 5*C* pyrrhotite is disordered along the **b**-axis, similar to that in the 6*C* pyrrhotite. It also confirms that the vacancy exclusion principle, from which previous trial structures were derived, holds within a close-packed layer. In a chosen layer, the partially occupied iron sites are always surrounded by fully occupied or almost fully occupied iron sites. There are, however, no fully vacant sites in either this structure or the 6*C* structure. The partially occupied iron sites project on top of each other in groups along the **b**-axis, but the sum of the site occupation factors for each group implies that the exclusion principle holds locally between atoms in adjacent layers, i.e., the vacancies are probably adjacent to filled sites, but in a disordered arrangement along the **b**-axis.

No correlation could be found between the occupancy of the iron sites and the average iron to sulfur distances, the octahedral volumes or the quadratic elongation (Robinson et al. 1971).

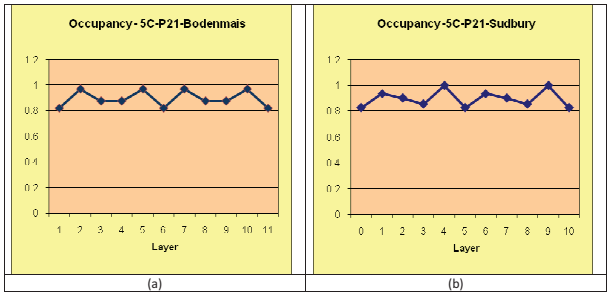

Figure 5. The layer occupancies in (**a**) the Bodenmais and (**b**) the Sudbury 5*C* pyrrhotite structures.

In the room-temperature Bodenmais structure, the iron to iron distances between the adjacent three partially occupied sites [Fe12-Fe19 of 2.71(2) Å and Fe19-Fe14 of 2.76(2) Å] are smaller than those between fully occupied sites [2.869(4)–2.965(4) Å] and this also correlates with the relatively large atomic displacement parameter of Fe19, even in the 120 K refinement. Smaller iron to iron distances of 2.603(8) Å are also present between the half occupied Fe2 and Fe9 sites in the room-temperature structure.

Finally, the layer occupancies in the two structures are shown in Figure 5. The Bodenmais arrangement is very similar to that of the orthorhombic structure described by de Villiers et al. (2009). This confirms the observations that it is difficult to derive the correct vacancy distribution of the intermediate pyrrhotites in these pseudosymmetric structures.

Acknowledgments

The microprobe analyses done by Peter Gräser are gratefully acknowledged. A special thanks to Kilian Pollok and Dennis Harries of the University of Bayreuth for the provision of excellent quality samples. Grateful thanks to Oxford Diffraction (Agilent Technologies) and Andy Dorn for making available their in-house diffraction facilities (Yarnton, Oxford, U.K.) and to Zoltán Gál for the low-temperature data collection for the Bodenmais crystal. Again, Alison Tuling provided help with graphic challenges. The comments and suggestions of two reviewers and the associate editor, which improved the manuscript substantially, are acknowledged.

References cited

Bruker (2001) SAINT+ Version 6.45, SADABS Version 2.10, SHELXTS and SHELXTL Version 6.14. BRUKER AXS Inc., Madison, Wisconsin.

Clark, R.C. and Reid, J.S. (1995) The analytical calculation of absorption in multifaceted crystals. Acta Crystallographica, A51, 887–897.

de Villiers, J.P.R. and Liles, D.C. (2010) The crystal-structure and vacancy distribution in 6*C* pyrrhotite. American Mineralogist, 95, 148–152.

de Villiers, J.P.R., Liles, D.C., and Becker, M. (2009) The crystal structure of a naturally occurring 5*C* pyrrhotite from Sudbury, its chemistry, and vacancy distribution. American Mineralogist, 94, 1405–1410.

Elliott, A.D. (2010) Structure of pyrrhotite 5C (Fe_9S_{10}). Acta Crystallographica, B66, 271–279.

Oxford Diffraction (2010) CrysAlisPro, version 1.171.34.41 (release 13-09-2010 CrysAlis171 .NET). Oxford Diffraction, Abingdon, U.K.

Robinson, K., Gibbs, G.V., and Ribbe, P.H. (1971) Quadratic Elongation: A quantitative measure of distortion in coordination polyhedra. Science, 72, 567–570.

Sheldrick, G.M. (2008) A short history of SHELX. Acta Crystallographica, A64, 112–122.

Wang, H. and Salveson, I. (2005) A review on the mineral chemistry of the non-stoichiometric iron sulphide, $Fe_{1-x}S$ ($0 \le x \le 0.125$): polymorphs, phase relations and transitions, electronic and magnetic structures. Phase Transitions, 78, 547–567.

Manuscript received May 17, 2011
Manuscript accepted October 9, 2011
Manuscript handled by Alexandra Friedrich